LUND UNIVERSITY

Accurate and efficient evaluation of modal Green's functions

Gustafsson, Mats

2010

[Link to publication](#)

Total number of authors:
1

Accurate and efficient evaluation of modal Green's functions

Mats Gustafsson

Mats Gustafsson
Mats.Gustafsson@eit.lth.se

Department of Electrical and Information Technology
Electromagnetic Theory
Lund University
P.O. Box 118
SE-221 00 Lund
Sweden

Abstract

Accurate and efficient numerical evaluations of the modal Green's functions are essential in radar cross section, scattering, and antenna problems involving bodies of revolution. It is shown that a combination between the trapezoidal rule and Gauss-Hermite quadrature along the steepest-decent contours produce 10 digits of accuracy for a low computational cost in non-singular cases. The near singular cases are of similar accuracy for a slightly higher computational cost.

1 Introduction

The integral equations in electromagnetics and acoustics for bodies of revolution require evaluation of modal Green's functions. This is useful in radar cross section computations where the scattered field is decomposed into Fourier modes [2, 8, 9]. It is particular efficient for the extinction cross section in the axial direction where only the first order modes are needed [12]. The approach is also used in inverse source problems where the integral equation and integral representation are inverted [10, 11].

Modal Green's functions simplify the solution of integral equations for bodies of revolution by reducing the integral equation one spatial dimension [2, 8, 9]. Surface integral equations (two dimensional) are hence reduced to line integral equations (one dimensional). This improves speed, reduce memory requirements, and simplify meshing. The drawback is that the original simple free-space Green's function, $\exp(-\mathrm{i}kR)/R$, is replaced by the modal Green's functions that involve weighted integrals of the free-space Green's function. This integration increases the computational cost and reduces the accuracy of the integral equation unless the modal Green's functions are evaluated with high accuracy at a low computational cost. Note, that the number of evaluations of the modal Green's function scale as k^2 for large wavenumbers k when used in the solution of integral equations. It is hence essential that the computational cost to evaluate them does not increase with k.

Various approaches can be used to compute the modal Green's functions. The fast Fourier transform (FFT) is used for simultaneous evaluation of all order of the modal Green's functions [6]. Series expansions are considered in [1]. In [13], an approximation using Bessel functions is suggested for near axial points.

In this paper, it is shown that the modal Green's functions can be evaluated accurately for a fixed computational cost. The computational challenges are due to oscillatory and/or singular integrals. The computation of the modal Green's functions are divided into four cases depending on their arguments; 1) weakly oscillatory integrals, 2) weakly oscillatory singular integrals, 3) oscillatory integrals, 4) oscillatory singular integrals. The first case is accurately evaluated with the trapezoidal rule, *e.g.*, 10 digits with 10 evaluations, due to the periodicity [5]. The second singular case is computed with subtraction of the static term using elliptic integrals [4]. The third case is the most common case on many objects and it is evaluated using Gauss-Hermite quadrature [5, 7] along the steepest-decent contours [3]

with *e.g.*, 10 digits for between 6 and 20 evaluation points. Finally, the fourth case is evaluated using Gauss-Hermite quadrature along one steepest-decent contour and Gauss-Laguerre quadrature after subtraction of analytically integrated parts.

2   The modal Green's functions

The modal Green's functions are commonly used in integral equations for scattering and antenna problems involving bodies of revolution. They are defined in a cylindrical coordinate system with the axis of revolution z, radius $\rho = \sqrt{x^2 + y^2}$, and azimuthal angle ϕ defined such that $x = \rho \cos \phi$, see Fig. 1.

Three modal Green's functions are used in electromagnetics [13]. They are

$$g_m = \int_0^\pi \frac{\mathrm{e}^{-\mathrm{i}kR}}{R} \cos m\phi \, \mathrm{d}\phi \tag{2.1}$$

$$g_{\mathrm{c},m} = \int_0^\pi \frac{\mathrm{e}^{-\mathrm{i}kR}}{R} \cos m\phi \cos \phi \, \mathrm{d}\phi \tag{2.2}$$

$$g_{\mathrm{s},m} = \int_0^\pi \frac{\mathrm{e}^{-\mathrm{i}kR}}{R} \sin m\phi \sin \phi \, \mathrm{d}\phi \tag{2.3}$$

where $R = \sqrt{\rho^2 + \rho'^2 - 2\rho\rho' \cos \phi + (z - z')^2}$, k denotes the wavenumber, and m is a non-negative integer. Introduce the parameters $R_0 = (\rho^2 + \rho'^2 + (z - z')^2)^{1/2} \geq 0$, $0 \leq \alpha = \rho_0^2/R_0^2 \leq 1$, and $\rho_0 = \sqrt{2\rho\rho'} \geq 0$ to rewrite (2.1) as

$$g_m = \frac{1}{R_0} \int_0^\pi \frac{\mathrm{e}^{-\mathrm{i}kR_0\sqrt{1-\alpha\cos\phi}}}{\sqrt{1 - \alpha \cos \phi}} \cos m\phi \, \mathrm{d}\phi. \tag{2.4}$$

and similarly for $g_{\mathrm{c},m}$ and $g_{\mathrm{s},m}$. The major difficulties in the numerical integration of (2.4) are due to the singularity of the integrand at $\phi = 0$ if $\alpha \approx 1$ and the rapid oscillations of the integrand for large values of kR_0. The following presentation is focused on g_1, but the results are also valid for g_m as well as $g_{\mathrm{c},m}$ and $g_{\mathrm{s},m}$. Integration of $g_{\mathrm{s},m}$ is in general simpler as the $\sin \phi$ term cancels the singularity. It is convenient to introduce the parameters $\Delta = \sqrt{(\rho - \rho')^2 + (z - z')^2}$ and $\beta_\mp = \sqrt{1/\alpha \mp 1}$ to quantify the distance to the singularity, note that $\beta_- = \Delta/\rho_0$, see also Fig. 1c.

3   Trapezoidal rule

The trapezoidal rule is very efficient for smooth periodic functions [5]. Although, the integrand in (2.4) is not periodic in $[0, \pi]$ it is observed that it is half of the corresponding extended periodic function in $[0, 2\pi]$. The trapezoidal rule is hence suitable if the derivatives of the integrand are bounded. This excludes the singular point $\alpha = 1$ as well as near singular points $\alpha \approx 1$. The accuracy depends on the number of sample points. As seen in Fig 2, where 10 equidistant samples are used, the accuracy is good for values such that $kR_0\alpha < 8$. The increasing errors for large $kR_0\alpha$ are due to the insufficient sampling of the integrand that oscillates as
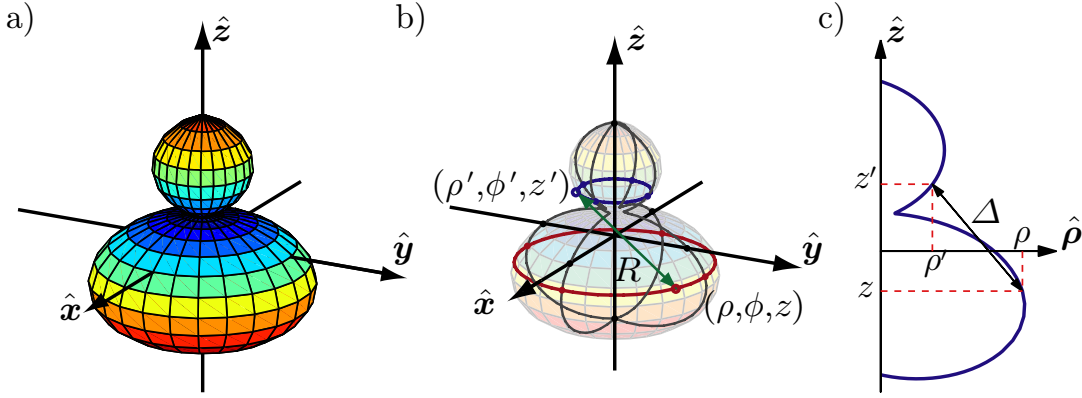
Figure 1: Geometry of a body of revolution. a) object. b) distance R between two points with coordinates $\boldsymbol{r}$ and $\boldsymbol{r}'$. c) object as function of the radius ρ and height z with distance Δ.

$kR_0\alpha/2 + m$. Larger $kR_0\alpha$ require additional sample points in the trapezoidal rule with an associated increased computational cost.

Integration of the near terms $\beta_- = \Delta/\rho_0 \ll 1$ improves by subtraction of the static contribution, *i.e.*, analytic integration of the integral

$$\int_0^\pi \frac{\mathrm{d}\phi}{\sqrt{1 - \alpha\cos\phi}} = \frac{2}{\sqrt{1+\alpha}}\mathrm{K}\left(\sqrt{\frac{2\alpha}{1+\alpha}}\right), \tag{3.1}$$

where K denotes the complete elliptic integral [4]. The relative error of the trapezoidal rule using 200 equidistant sample points together with subtraction of the static term (3.1) is depicted in Fig. 2b. Here, it is observed that the accuracy is improved for large kR_0 due to the dense sampling as well as for the near singular points or small values for kR_0 due to the extraction of the singularity. The relative error is easily decreased by even denser sampling. This is of no practical problem for small kR_0 but it is not feasible for large kR_0.

4 Steepest decent contours

The integrand (2.4) is analytic in ϕ for $0 < \mathrm{Re}\,\phi < \pi$ so the Cauchy integral theorem [3] can be used to deformation the integration contour to complex valued ϕ. Consider a deformation of the integration interval $[0, \pi]$ to $\gamma_1 + \gamma_2$ as depicted in Fig. 3a. The integral is then divided into the two parts

$$g_m R_0 = \int_{\gamma_1} \frac{\mathrm{e}^{-\mathrm{i}kR}}{R/R_0}\cos m\phi\,\mathrm{d}\phi + \int_{\gamma_2} \frac{\mathrm{e}^{-\mathrm{i}kR}}{R/R_0}\cos m\phi\,\mathrm{d}\phi, \tag{4.1}$$

where the Green's function is scaled with R_0 for notational simplicity. Use that $\mathrm{e}^{-\mathrm{i}kR}$ decays exponentially if $\mathrm{Im}\,R < 0$. This requires $\mathrm{Im}\{\cos\phi\} > 0$ or equivalently $\mathrm{Im}\,\phi < 0$ for $0 \le \mathrm{Re}\,\phi \le \pi$. It is preferable to use the steepest decent contours
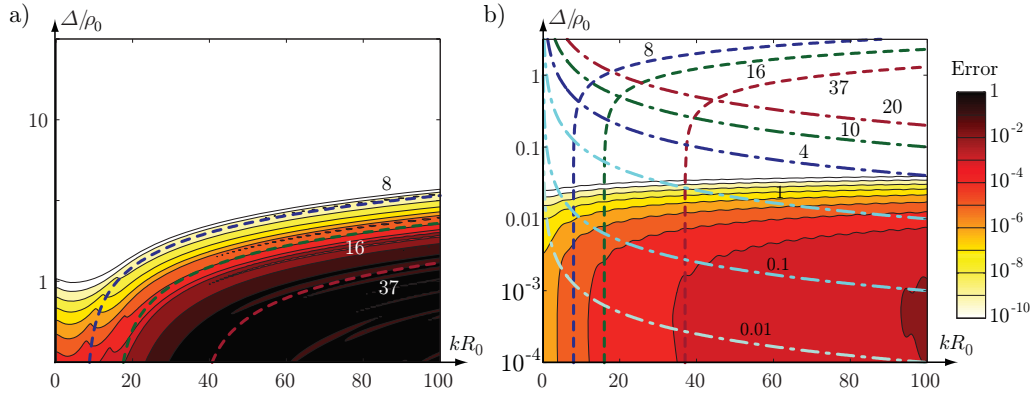
Figure 2: Contour plots depicting the relative error of g_1 for a) the 10 point trapezoidal quadrature rule and b) 200 point trapezoidal quadrature rule with extraction of the static term. The dashed curves, defined by $kR_0\alpha = 8, 16, 37$, illustrate the regions of approximation due to the oscillations of the integrand. The dashed dotted lines, defined by $k\Delta = 20, 10, 4, 1, 0.1, 0.01$, illustrate the regions of approximation due to the singularity.

where the integrands do not oscillate. These contours are defined by

$$\mathrm{Re}\, R/R_0 = \mathrm{Re}\,\sqrt{1 - \alpha(x + iy)} = \sqrt{1 \mp \alpha}, \tag{4.2}$$

where $\cos\phi = x + iy$ and the $\mp$ signs correspond to the contours γ_1 and γ_2 as depicted in Fig. 3a.

Use that the real-valued part of the square root (4.2), see (A.1), can be rewritten

$$2(\mathrm{Re}\, R/R_0)^2 = \sqrt{(1 - \alpha x)^2 + \alpha^2 y^2} + 1 - \alpha x = 2(1 \mp \alpha). \tag{4.3}$$

This is further simplified in several steps as $(1 - \alpha x)^2 + \alpha^2 y^2 = (1 - \alpha(2 \mp x))^2$ and $\alpha^2 y^2 = (1 - \alpha(2 \mp x))^2 - (1 - \alpha x)^2$ that finally gives the steepest decent contours

$$x = \frac{y^2}{4(1/\alpha \mp 1)} \pm 1 = \frac{y^2}{4\beta_\mp^2} \pm 1. \tag{4.4}$$

It observed that $x > 1$ and $x > -1$ in the first and second cases, respectively, see Fig.3b. The decay along the steepest decent path is given by the corresponding imaginary part of R/R_0, that is written

$$(\mathrm{Im}\, R/R_0)^2 = (\sqrt{(1 - \alpha x)^2 + \alpha^2 y^2} - 1 + \alpha x)/2$$
$$= (1 \mp \alpha(2 \mp x) - 1 + \alpha x)/2 = \frac{\alpha}{4\beta_\mp^2} y^2. \tag{4.5}$$

The normalized distance R/R_0 is hence simply

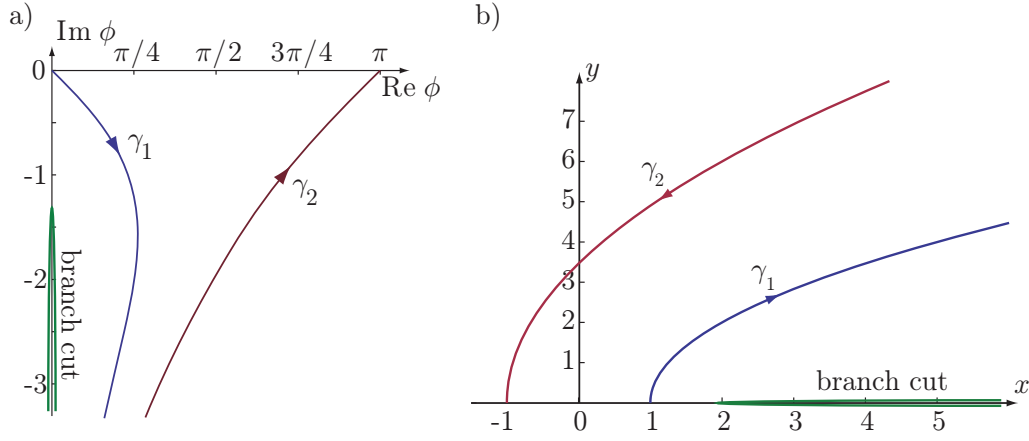$$R/R_0 = \left(\sqrt{1 \mp \alpha} - i\sqrt{\alpha(x \mp 1)}\right) = \sqrt{\alpha}(\beta_\mp - i\frac{y}{2\beta_\mp}) \tag{4.6}$$

Figure 3: Integration contours γ_1 and γ_2 for $\alpha = 1/2$. a) in the complex valued ϕ plane. b) in the $x + iy = \cos\phi$ plane as given by (4.4).

along γ_{12}, where it is observed that the integrand decays exponentially in y. Integration along γ_{12} require the change of variables $z = x + iy = \cos\phi$ that gives $-\sin\phi\,d\phi = dz$ and it is parameterized in y as

$$dz = dx + i\,dy = (\frac{dx}{dy} + i)\,dy = (\frac{y}{2\beta_\mp^2} + i)\,dy. \tag{4.7}$$

The trigonometric functions in the modal Green's functions (2.1) and variable substitution above are evaluated on the γ_{12} contours as

$$\cos\phi = x + iy = x + i2\sqrt{x \mp 1}\beta_\mp = \frac{y^2}{4\beta_\mp^2} \pm 1 + iy \tag{4.8}$$

and

$$\sin\phi = \sqrt{1 - (x + iy)^2} = \sqrt{1 - x^2 + y^2 - 2ixy}$$

$$= \sqrt{-\frac{y^2}{4\beta_\mp^2}(2 \pm \frac{y^2}{4\beta_\mp^2}) + y^2 - 2iy(\frac{y^2}{4\beta_\mp^2} \pm 1)}. \tag{4.9}$$

The integrand is finally simplified with the substitution $\tau^2 = y/2\beta_\mp$, that gives

$$R/R_0 = \sqrt{\alpha}(\beta_\mp - i\tau^2) = -i\sqrt{\alpha}(\tau^2 + i\beta_\mp) \tag{4.10}$$
$$dz = (1 + i\beta_\mp/\tau^2)\,dx = 4(\tau^2 + i\beta_\mp)\tau\,d\tau \tag{4.11}$$
$$\cos\phi = \tau^4 \pm 1 + i2\tau^2\beta_\mp \tag{4.12}$$
$$\sin\phi = \tau\sqrt{-\tau^6 + (4\beta_\mp^2 \mp 2)\tau^2 - i4\beta_\mp(\tau^4 \pm 1)}, \tag{4.13}$$

where it is noted that the variable substitution cancels the $1/R$ term.

The integrals (4.1) are

$$-\,\mathrm{e}^{-\mathrm{i}kR_0\sqrt{1\mp\alpha}}\int_\gamma \frac{\mathrm{e}^{-kR_0\sqrt{\alpha}\tau^2}}{R/R_0}\frac{\cos\phi}{\sin\phi}\,\mathrm{d}z$$

$$=4\frac{\mathrm{e}^{-\mathrm{i}k\rho_0\beta_\mp}}{\sqrt{\alpha}}\int_0^\infty \frac{\mathrm{e}^{-k\rho_0\tau^2}\big(\tau^4\pm1+\mathrm{i}2\tau^2\beta_\mp\big)}{\sqrt{-\tau^6+(4\beta_\mp^2\mp2)\tau^2-\mathrm{i}4\beta_\mp(\tau^4\pm1)}}\,\mathrm{d}\tau. \quad (4.14)$$

These integrals are well defined. However, the convergence deteriorates for small $k\rho_0$ and it has a $1/\tau$ singularity in the $\beta_-\to0$ limit. Note, that $\beta_+\geq1$ on γ_2 but $\beta_-=\Delta/\rho_0\to0$ as $\Delta\to0$ on γ_1, where Δ denotes the distance between the evaluation points, see Fig. 1c.

4.1 Gauss-Hermite quadrature

Evaluate the integrals (4.14) using Gauss-Hermite quadrature [5], where the normal form

$$I_\mp=\int_0^\infty \mathrm{e}^{-k\rho_0\tau^2}f_\mp(\tau)\,\mathrm{d}\tau=\int_0^\infty \frac{\mathrm{e}^{-\tau^2}f_\mp(\tau/\sqrt{k\rho_0})}{\sqrt{k\rho_0}}\,\mathrm{d}\tau, \quad (4.15)$$

is used and where

$$f_\mp(\tau)=\frac{\tau^4\pm1+\mathrm{i}2\tau^2\beta_\mp}{\sqrt{-\tau^6+(4\beta_\mp^2\mp2)\tau^2-\mathrm{i}4\beta_\mp(\tau^4\pm1)}}. \quad (4.16)$$

The integrals are approximated as

$$\int_0^\infty \mathrm{e}^{-k\rho_0\tau^2}f_\mp(\tau)\,\mathrm{d}\tau\approx\frac{1}{\sqrt{k\rho_0}}\sum_{n=1}^N w_n f_\mp(x_n/\sqrt{k\rho_0}), \quad (4.17)$$

where x_n and w_n are the zeros and weighting coefficients in the Gauss-Hermite quadrature with $x_n\geq0$. Here, the 10, 5, 3 point approximations are considered. The relative error of g_1 is depicted in Fig. 4a for the 10 point case as function of kR_0 and $\beta_-=\Delta/\rho_0$. It is observed that the errors are small for large kR_0 and $\Delta/\rho_0\approx1$. More specifically, the errors increase for small $kR_0\alpha$. This corresponds to slowly oscillating integrands and they are instead easily integrated by the trapezoidal rule as seen in Sec. 3. The relative error of the 10 point Gauss-Hermite quadrature is less than 10^{-10} for $kR_0\alpha>8$. The corresponding results for the 5 and 3 point approximations are given by $kR_0\alpha>16$ and $kR_0\alpha>37$, respectively. It is also required that the $k\Delta$ is sufficiently large, *i.e.*, the evaluation points should be separated of the order of a wavelength, $\lambda=2\pi/k$. In the figure it is seen that $k\Delta\geq4,10,20$ are sufficient for the 10, 5, 3 point approximations, respectively.

4.2 Near singular terms

The Gauss-Hermite quadrature is not efficient for the integral along γ_1 in the small β_- limit, *i.e.*, the singular case where $\alpha\approx1$ as seen in Fig. 4a. The problems are
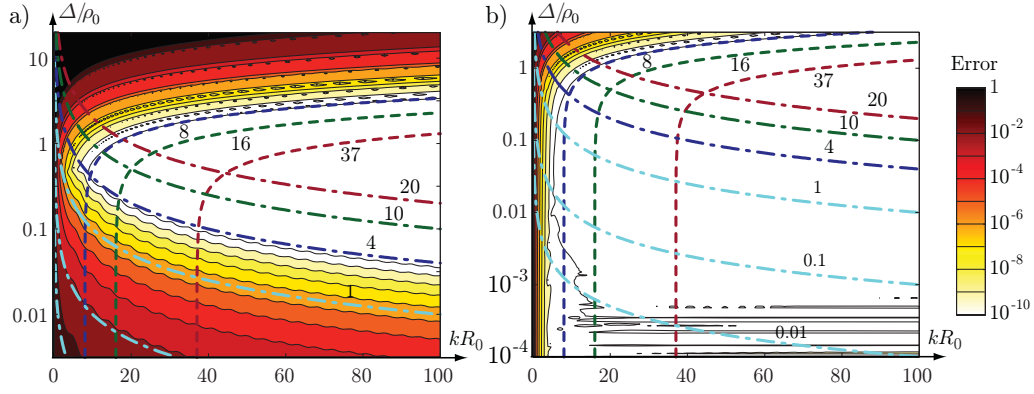
Figure 4: Contour plots of the relative errors for the Gauss quadrature of g_1. The dashed curves defined by $kR_0\alpha = 8, 16, 37$ illustrate the regions of approximation due to the oscillations of the integrand. The dashed dotted lines defined by $k\Delta = 20, 10, 4, 1, 0.1, 0.01$ illustrate the regions of approximation due to the singularity. a) 10 point Gauss-Hermite quadrature. b) 10 point Gauss-Hermite quadrature together with the near-singular corrections (4.22) and (4.23).

due to the increasing difficulties to approximate the square root with polynomials for small values of β_-. This requires more involved quadrature methods.

Divide the integration interval $[0, \infty]$, into $[0, \tau_1]$ and $[\tau_1, \infty]$, where the parameter τ_1 is determined below. The term $-4\beta_- - (2 - 4\beta_-^2)\tau^2$ dominates the square root in (4.16) as $\tau \to 0$. This part is extracted and integrated analytically. That is

$$I_{-0,[0,\tau_1]} = \int_0^{\tau_1} \frac{\mathrm{e}^{-k\rho_0\tau^2}}{\sqrt{-(2 - 4\beta_-^2)\tau^2 - \mathrm{i}4\beta_-}}\, \mathrm{d}\tau$$

$$= \frac{-\mathrm{i}}{\sqrt{(2 - 4\beta_-^2)}\sqrt{k\rho_0}} \int_0^{\tau_1\sqrt{k\rho_0}} \frac{\mathrm{e}^{-\tau^2}}{\sqrt{\tau^2 + \mathrm{i}\frac{2\beta_- k\rho_0}{1 - 2\beta_-^2}}}\, \mathrm{d}\tau, \quad (4.18)$$

where the integration variable is scaled with $\sqrt{k\rho_0}$. The singularity dominates if $2\beta_- k\rho_0/(1 - 2\beta_-^2) \approx 2k\Delta \ll 1$. Use the Taylor series expansion

$$\mathrm{e}^{-k\rho_0\tau^2} = \sum_{n=0}^{\infty} (-1)^n \frac{k^n \rho_0^n \tau^{2n}}{n!} \tag{4.19}$$

together with the identity

$$\int \frac{1}{\sqrt{a\tau^2 + b}}\, \mathrm{d}\tau = \frac{1}{\sqrt{a}} \ln(\tau\sqrt{a} + \sqrt{a\tau^2 + b}) \tag{4.20}$$

and the recursions

$$\int \frac{\tau^n}{\sqrt{a\tau^2 + b}}\, \mathrm{d}\tau = \frac{\tau^{n-1}\sqrt{a\tau^2 + b}}{na} - \frac{(n-1)b}{na} \int \frac{\tau^{n-2}}{\sqrt{a\tau^2 + b}}\, \mathrm{d}\tau \tag{4.21}$$

to integrate (4.18). This quadrature rule is simple and efficient if $|b| < |a|$. The total integral over $[0, \tau_1]$ is then

$$I_{-,[0,\tau_1]} = \int_0^{\tau_1} \mathrm{e}^{-k\rho_0\tau^2}\left(f_-(\tau) - \frac{1}{\sqrt{(4\beta_-^2 - 2)\tau^2 - \mathrm{i}4\beta_-}}\right)\mathrm{d}\tau + I_{-0,[0,\tau_1]}. \qquad (4.22)$$

Here, $I_{-0,[0,\tau_1]}$ is computed with the recursions (4.21) together with (4.20). The reminding integrand is smooth and Gauss quadrature [5] is used below. The rest of the integral is

$$I_{-,[\tau_1,\infty]} = \int_{\tau_1}^{\infty} \mathrm{e}^{-k\rho_0\tau^2} f_-(\tau)\,\mathrm{d}\tau = \int_{\tau_1^2}^{\infty} \frac{\mathrm{e}^{-k\rho_0 t} f_-(\sqrt{t})}{2\sqrt{t}}\,\mathrm{d}t$$

$$= \mathrm{e}^{-k\rho_0\tau_1^2} \int_0^{\infty} \frac{\mathrm{e}^{-k\rho_0 t} f_-(\sqrt{t + \tau_1^2})}{2\sqrt{t + \tau_1^2}}\,\mathrm{d}t. \quad (4.23)$$

Numerical quadrature of this integral can be performed by Gauss-Laguerre quadrature [5]. It is observed that an appropriate choice of the parameter τ_1 is essential. Quadrature of (4.22) simplifies for small τ_1 as the effects of the neglected higher order terms in (4.18) reduce. On the contrary, the square root dominates (4.23) for small τ_1 with increasing difficulty to use Gauss-Laguerre quadrature. It is found that $\tau_1 \approx 1.5/\sqrt{k\rho_0}$ offers a good compromise. The resulting relative error is depicted in Fig. 4b where 20 and 16 quadrature points are used in (4.22) and (4.23), respectively.

5 Conclusions

An approach for accurate and efficient evaluation of the modal Green's functions is presented. The non-singular oscillatory case is transformed to its steepest decent paths and integrated using Gauss-Hermite quadrature. This is the most common situation for electrically large objects and reduces the computational cost to between 6 and 20 function evaluations. The singular oscillatory case is more involved. Here, the integral is divided into an analytically integrated part and two parts that are integrated with Gauss quadrature. This requires approximately 40 function evaluations. The modal Green's functions for $m = 1$ are used to illustrate the results. This is particular useful for evaluation of the extinction cross section [12].

Acknowledgment

Appendix A   Square root of a complex number

The square root of a complex number, $a + \mathrm{i}b$, with negative imaginary part $(b < 0)$ is

$$\sqrt{a + \mathrm{i}b} = \sqrt{\frac{\sqrt{a^2 + b^2} + a}{2}} - \mathrm{i}\sqrt{\frac{\sqrt{a^2 + b^2} - a}{2}} \qquad (A.1)$$

References

[1] A. K. Abdelmageed. Efficient evaluation of modal Green's functions arising in EM scattering by bodies of revolution. *Progress In Electromagnetics Research*, **27**, 337–356, 2000.

[2] M. Andreasen. Scattering from bodies of revolution. *IEEE Trans. Antennas Propagat.*, **13**(2), 303–310, 1965.

[3] G. Arfken. *Mathematical Methods for Physicists*. Academic Press, Orlando, third edition, 1985.

[4] A. Bondeson, T. Rylander, and P. Ingelström. *Computational Electromagnetics*. Springer-Verlag, Berlin, 2005.

[5] P. J. Davis and P. Rabinowitz. *Methods of numerical integration*. Academic Press, New York, 1975.

[6] S. D. Gedney and R. Mittra. The use of the FFT for the efficient solution of the problem of electromagnetic scattering by a body of revolution. *IEEE Trans. Antennas Propagat.*, **38**(3), 313–322, 1990.

[7] D. Huybrechs and S. Vandewalle. On the evaluation of highly oscillatory integrals by analytic continuation. *SIAM Journal on Numerical Analysis*, **44**(3), 1026–1048, 2007.

[8] J. R. Mautz and R. F. Harrington. Radiation and scattering from bodies of revolution. *Appl. Scientific Research*, **20**(1), 405–435, 1969.

[9] J. R. Mautz and R. F. Harrington. Electromagnetic scattering from a homogeneous material body of revolution. *Archiv für Elektronik und Übertragungstechnik (AEÜ)*, **33**, 71–80, 1979.

[10] S. Nordebo, M. Gustafsson, and K. Persson. Sensitivity analysis for antenna near-field imaging. *IEEE Trans. Signal Process.*, **55**(1), 94–101, January 2007.

[11] K. Persson and M. Gustafsson. Reconstruction of equivalent currents using a near-field data transformation – with radome applications. *Progress in Electromagnetics Research*, **54**, 179–198, 2005.

[12] C. Sohl, M. Gustafsson, and G. Kristensson. Physical limitations on broadband scattering by heterogeneous obstacles. *J. Phys. A: Math. Theor.*, **40**, 11165–11182, 2007.

[13] W. M. Yu, D. G. Fang, and T. J. Cui. Closed form modal Green's functions for accelerated computation of bodies of revolution. *IEEE Trans. Antennas Propagat.*, **56**(11), 3452–3461, 2008.